Solid State Ionics 326 (2018) 116–123

Contents lists available at ScienceDirect

Solid State Ionics

journal homepage: www.elsevier.com/locate/ssi

Study of $La_4BaCu_{5-x}Co_xO_{13+\delta}$ series as potential cathode materials for intermediate-temperature solid oxide fuel cell

Silvia Duran[a,b], Jhoan Tellez[a,b], Mónica V. Sandoval[a], Mario A. Macias[a,c], Edouard Capoen[d], Caroline Pirovano[d], Pascal Roussel[d], Anna Niemczyk[e], Mónica Barrera Castillo[f], Liliana Mogni[f], Leopoldo Suescun[b], Gilles H. Gauthier[a,*]

[a] Universidad Industrial de Santander, INTERFASE, Bucaramanga, Colombia
[b] Universidad de la República, Facultad de Química, Cryssmat-Lab/DETEMA, Montevideo, Uruguay
[c] Universidad de los Andes, Departamento de Química, Bogotá, Colombia
[d] Université. Lille, CNRS, Centrale Lille, ENSCL, Univ. Artois, UMR 8181 - UCCS - Unité de Catalyse et Chimie du Solide, F-59000 Lille, France
[e] AGH University of Science and Technology, Faculty of Energy and Fuels, Krakow, Poland
[f] Centro Atómico Bariloche, Instituto Balseiro, Comisión Nacional de Energía Atómica, Av. Bustillo 9500, 8400 S. C. de Bariloche, Argentina

ARTICLE INFO

Keywords:
SOFC
Perovskite
Cathode
Cobaltocuprate
Electrical conductivity
Electrochemical impedance spectroscopy

ABSTRACT

$La_4BaCu_{5-x}Co_xO_{13+\delta}$ system was successfully synthesized by a modified Pechini route in air. A structural phase transition is observed along the series, from tetragonal ordered structure for $0 \le x \le 2$ to a rhombohedral disordered perovskite for $x = 5$. A TEC value of $17.3 \times 10^{-6}\,K^{-1}$, was found by High-Temperature X-ray Diffraction (HT-XRD) in air for $La_4BaCu_3Co_2O_{13+\delta}$. The conductivity of $La_4BaCu_3Co_2O_{13+\delta}$ increases with temperature reaching a maximum of $778\,S\,cm^{-1}$ at 405 °C in air followed by a decrease with further increase in temperature with values of 600–664 $S\,cm^{-1}$. The cathode polarization resistance of $La_4BaCu_3Co_2O_{13+\delta}$ evaluated in air at 750 °C is $0.34\,\Omega\,cm^2$ with an activation energy of 1.65 eV. These results demonstrate the possible use of $La_4BaCu_{5-x}Co_xO_{13+\delta}$ materials as cathode for Intermediate-Temperature Solid Oxide Fuel Cell (IT-SOFC).

1. Introduction

Developing alternative sources of energy that may at some point replace the traditional ones has made new technologies like the Solid Oxide Fuel Cells (SOFC) emerge due to their ability to use a wide variety of fuels with a high theoretical level of energy conversion efficiency and low greenhouse gas emission [1,2]. However, the high temperature of operation remains one of the main issues of SOFC developments because of cell materials degradation [3]. For this reason, the scientific community working on the topic is focused on the search for new electrochemically active materials that can operate at lower temperature (T < 700 °C) and can contribute to the improvement of the so-called IT-SOFCs (IT for "Intermediate Temperature") [4]. Materials such as Rare Earth cobaltites of perovskite (or derived) structure result as attractive compounds for use as IT-SOFC cathodes, mainly due to their possible oxygen deficiency, especially at high temperature [5–8]. However, some of these materials have shown mechanical incompatibilities with the electrolytes due to elevated thermal expansion coefficients caused by a strong variation of oxygen content with temperature. A solution has been found by adequate substitution of cobalt, for example with iron, which mitigates the high chemical and thermal expansion. The $La_{1-x}Sr_xFe_{1-y}Co_yO_{3-\delta}$ cobaltoferrites present a good ionic and electronic conduction, as well as a good chemical and thermal compatibility with CeO_2-based electrolytes [9]. Rare Earth-free cobaltoferrites of cubic perovskite structure have been also proposed as IT-SOFC cathode, such as $Ba_{0.5}Sr_{0.5}Co_{0.8}Fe_{0.2}O_3$ (BSCF), with very interesting performance for cells operating at temperature as low as 600 °C [10]. Unfortunately, the chemical stability is an issue for those materials for temperatures below 850 °C [11]. Recently, perovskites having oxygen vacancy ordering have been proposed as interesting alternatives to classical disordered perovskites like LSCF or BSCF; this is the case of $REBaCo_2O_{5+\delta}$ (RE = Rare Earth) materials, in which RE and Ba cations occupy the A-site perovskite sub-lattice and oxygen vacancies are localized within the LnO_δ layers, presenting high electrical conductivity and electrocatalytical activity for Oxygen Reduction Reaction (ORR) [12–16]. However, once again, the application of those pure cobaltite cathode materials is impeded by high thermal expansion coefficient (TEC). Various studies have demonstrated that $LnBaCo_{2-x}M_xO_{5+\delta}$ (Ln = Pr, Nd, Sm, Gd, M = Fe, Cu, Ni) oxides possess lower TEC values than $LnBaCo_2O_{5+\delta}$ [17–19]. For example, the TEC

* Corresponding author.
E-mail address: gilgau@uis.edu.co (G.H. Gauthier).

https://doi.org/10.1016/j.ssi.2018.10.001
Received 29 August 2018; Received in revised form 26 September 2018; Accepted 2 October 2018

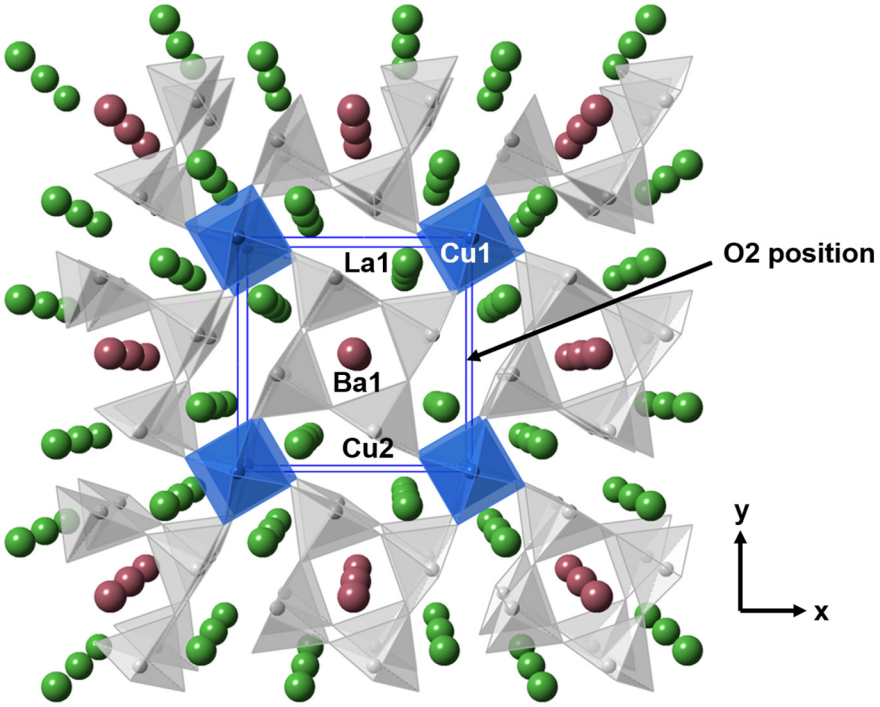

Fig. 1. Graphical representation along [001] of $La_4BaCu_5O_{13+\delta}$ (LBCu) showing the position of O2 atoms in the tunnel framework.

value for $SmBaCoCuO_{5+\delta}$ is $15.53 \times 10^{-6} K^{-1}$ from 30 °C to 850 °C, much lower than the $21.9 \times 10^{-6} K^{-1}$ at 700 °C for $SmBaCo_2O_{5+\delta}$ [19]. In the same family of oxygen vacancy ordered cuprocobaltites, the recently highlighted MIEC material $SmBa_{0.5}Sr_{0.5}CoCuO_{5+\delta}$ (SBSCCo) seems a very promising compromise between performance and compatibility with GDC or LSGM electrolytes, especially with respect to TEC values [20].

In a previous study, we demonstrated the interest to examine the case of another oxygen-vacancy-ordered family based on a cuprate structure of composition $La_4BaCu_5O_{13+\delta}$, thereinafter referred to as LBCu (Fig. 1) showing oxygen vacancy rows. This material is particularly stable until 900 °C, presents a good compatibility with yttrium-doped barium cerate-zirconate (BCZY) electrolyte, reasonable TEC value of $17.3 \times 10^{-6} K^{-1}$ and high electrical conductivity around 500 S cm^{-1}, making it of special interest as cathode material [21]. Nevertheless, very limited oxygen excess δ was evidenced in vacant sites below 700 °C in air in the pure cuprate and such structural feature is of importance for the MIEC behavior of the material. As a consequence, the present work concerns the synthesis and preliminary evaluation of Co substitution in $La_4BaCu_5O_{13+\delta}$, with the aim to possibly increase oxygen nonstoichiometry at high temperature in air. A second goal of our study is to compare in the future the cathode behavior of materials with ordered and disordered (cubic-like perovskite) structure, respectively, within the $La_4BaCu_{5-x}Co_xO_{13+\delta}$ series.

2. Experimental

$La_4BaCu_{5-x}Co_xO_{13+\delta}$ ($0 \le x \le 5$) compounds were synthesized using the polymeric gel method [22,23], an alternative route that has been shown very effective for the synthesis of the pure or Ni-doped cuprate [24,25], in comparison to the previous report of Anderson et al. on the same cobalt-doped series prepared by solid state reaction [26]. In this regard, stoichiometric amounts of CuO (≥99,9% Alfa Aesar), Co_3O_4 (≥99,9% Alfa Aesar), $BaCO_3$ (≥99,9% Aldrich), La_2O_3 (≥99,9% Alfa Aesar) were weighed and dissolved in the minimum quantity of water and HNO_3 (Sigma Aldrich 68.0–70.0%), before pouring the chelating agent Ethylene Diamine Tetraacetic acid (EDTA, ≥99.4% Sigma Aldrich) in a molar ratio of EDTA:(cation)$_{total}$ = 1:1 [27], adding NH_4OH (28.0–30.0% Sigma Aldrich) in order to dissolve the EDTA and maintain the pH value to 9–10. Citric acid (CA, ≥99,5% Merck) was also added in a molar ratio of EDTA:CA = 1:1.5 [28], necessary to make the complete dissolution of lanthanum oxide faster and obtain a homogeneous and stable solution. The resulting deep blue-purple solution was heated at 70–90 °C under constant stirring. Temperature was gradually increased until reaching 110 °C in order to evaporate the water and ethylene glycol (≥99% Panreac) was added in a proportion of 1.5 mL per gram of final product, initiating gel formation. The resulting viscous gel was subsequently heated at ~200 °C so that a dry dark gel was obtained, that was subsequently calcined around T = 300 °C then T = 500 °C for 3–4 h in air to ensure total organic matter decomposition and obtain ashes. Finally, the powder was grinded in an agate mortar and then pressed into pellets of 1 cm in diameter, to be then sintered in air at 900 °C for 8 h for x = 0 and 950 °C for 5 h for $1 \le x \le 5$. As an alternative route, gel autocombustion synthesis can be used, that can produce finer powders than the above-described technique, in which stoichiometric amounts of $Cu(CH_3COO)_2$ (≥99.0% Sigma-Aldrich), $Ba(NO_3)_2$ (≥99% Sigma-Aldrich), $La(NO_3)_3{\cdot}6H_2O$ (99.99% Aldrich) and $Co(NO_3)_2{\cdot}6H_2O$ (≥98% Sigma-Aldrich) is used, with the same chelating agent (EDTA, ≥99.4% Sigma Aldrich) in a molar ratio of EDTA:(cation)$_{total}$ = 1:1 [27] adding NH_4OH (28.0–30.0% Sigma Aldrich) to maintain the pH value to 9–10 and NH_4NO_3 as fuel (≥99% Sigma Aldrich), resulting in a much stronger exothermicity of the combustion. After mixing of the reagents, similar to the previous route, the viscous gel is subsequently heated at ~300–400 °C on a hot plate so that the combustion reaction takes place, resulting in an intense flame and self-sustained combustion and ashes production. The final heat treatment is the same as for the previously described sol-gel method. Such gel autocombustion technique was preferred for the sample preparation that were used for conductivity measurements.

After synthesis, X-ray powder diffraction (XRD) measurements were carried out to analyze the samples. The data were recorded using a RIGAKU ULTIMA IV diffractometer in a Bragg-Brentano type focusing geometry and a CuK$\alpha_{1,2}$ radiation that handled current conditions at 30 mA and voltage at 40 kV. The patterns were collected at room temperature in an angular range of 8–70° (2θ), using a 2θ step size of

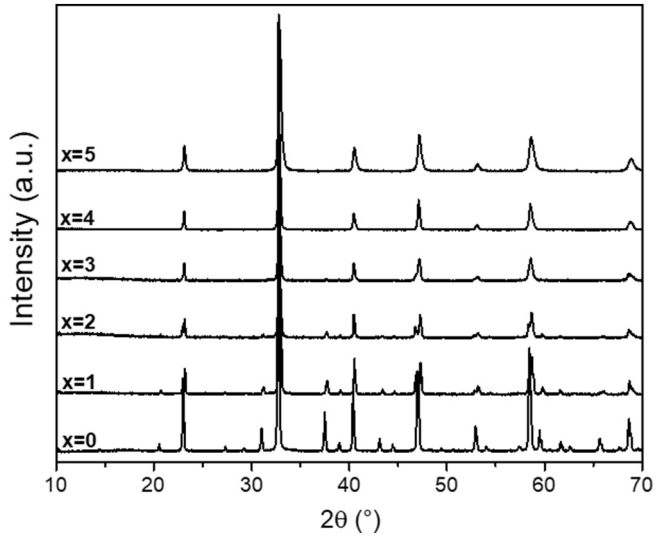

Fig. 2. X-ray powder diffraction patterns of $La_4BaCu_{5-x}Co_xO_{13+\delta}$ ($0 \le x \le 5$) after synthesis in air.

0.02°. XRPD patterns were refined using the Rietveld method, as implemented in the Fullprof program and its graphical interface WinPLOTR [29,30].

The structural properties of the materials were studied as a function of temperature in air with a special focus on $La_4BaCu_3Co_2O_{13+\delta}$ composition since it presents the same space group as LBCu (see below). HT-XRD (High Temperature – X Ray Diffraction) data were collected in air every 50 °C from Room Temperature (RT) to 850 °C using a Panalytical Empyrean diffractometer equipped with an Anton Paar HTK 1200 N oven chamber using a beam of $CuK\alpha_{1,2}$ radiation.

The evolution of the oxygen stoichiometry of $La_4BaCu_3Co_2O_{13+\delta}$ cobaltocuprate in air as a function of temperature was studied by thermogravimetric (TG) measurements in air, using a Discovery TGA 5500 gravimetric analyzer. Two cycles from RT to 800 °C were performed with a temperature ramp of 1.5 °C min^{-1} (the first cycle only for cleaning from adsorbed undesirable species). The absolute oxygen stoichiometry of the sample after synthesis was also determined by thermogravimetrical titration, using the complete decomposition of the sample up to 900 °C in 5%H_2/Ar (Linseis STA PT 1600 thermogravimetric analyzer, ramp rate of 1 °C min^{-1}) that results in the formation of La_2O_3, BaO, Cu and Co. For better accuracy, a preliminary cycle in air up to 800 °C with a ramp rate of 5 °C min^{-1} was performed, as in the case of TGA measurements in air.

In order to give a more precise insight into the structural evolution of $La_4BaCu_3Co_2O_{13+\delta}$ compound as function of temperature, especially with respect to oxygen atoms, neutron thermodiffraction experiments were performed in air from room temperature (RT) to 850 °C (5 °C min^{-1}) on the High Resolution Powder Diffractometer 3T2 using a wavelength of $\lambda = 1.225$ Å over the 2θ range from 3° to 120° and a step size of 0.05° at the LLB (*Laboratoire Léon Brillouin*), Saclay, France. The data analysis was performed by the Rietveld method using the Jana-2006 program [31].

The electrical conductivity measurements were performed using the 4-probe DC technique in a BioLogic SP-300 Potentiostat-Galvanostat from 50 °C to 800 °C with 50 °C step. Each powder was previously pressed in the form of dense cylindrical pellets (4 mm in diameter and 9 mm in thickness) and sintered at 1200 °C for 6 h leading to relative density higher than 70%. Gold wires and gold paste were used for electrical contacts. A direct current was injected through the two outside terminals, with values between 10 and 100 mA, and the voltage was measured between the two inside terminals. Conductivity values were corrected from porosity according to the empirical equation proposed in [32].

The electrochemical characterization was performed by impedance spectroscopy (IS) in a symmetrical cell configuration LBCuCo2/LSGM/LBCuCo2. Dense pellets of $La_{0.8}Sr_{0.2}Ga_{0.8}Mg_{0.2}O_{2.8}$ (LSGM) were made by pressing commercial powder of LSGM (FuelCell Materials-FCM) with 0.8%p/p of polyvinyl butyral (PVB) and sintered in air at 1200 °C for 12 h. Dense LSGM electrolytes of 500 µm were obtained. Spin coating technique was used to deposit cathode painting over both sides of the pellets. The inks were obtained by mixing 35% LBCuCo2 powder, 23.6% alpha-terpineol, 38.8% isopropyl alcohol, 1.7% PVB and 0.9% polyvinyl pyrrolidine (PVP), weight composition. The cells were calcined at 1000 °C for 3 h for cathode adhesion giving place to a uniformly porous LBCuCo2 cathode with an average 56(3) µm thickness. To check no chemical reaction takes place between LSGM and LBCuCo2, both materials were mixed in powder form and heat treated at 1050 °C during 24 h. XRD performed before and after treatment confirms no secondary phase formation (results not shown here).

Two series of measurements were collected by an AUTOLAB potentiostat PGSTAT30 (EcoChemie) with a frequency generator FRA2 module from 1 MHz to 0.1 mHz; AC signal amplitude of 50 mV. The first one in atmospheric air as a function of temperature (T) in the range of 500–750 °C. The second one at 700 °C as a function of O_2 gas partial pressure (pO_2) in an oxygen-argon controlled atmosphere (for pO_2 ranging from 0.001 to 1 atm). An electrochemical system formed by ZrO_2-based pump and sensor was used to control and measure the pO_2. Pt grids were used as current collectors. IS spectra were analyzed by using ZView software by adjusting electrical equivalent circuits.

3. Results and discussion

3.1. Structural analysis

The XRD patterns of the $La_4BaCu_{5-x}Co_xO_{13+\delta}$ materials for $0 \le x \le 5$ are shown in Fig. 2, after synthesis by the polymeric gel combustion technique in air. As in the case of x = 0 ($La_4BaCu_5O_{13+\delta}$), the X-ray diffractograms with x = 1 and 2 were successfully indexed with one single phase of tetragonal space group $P4/m$ with $a \sim \sqrt{5}a_p$ and $c \sim a_p$ (a_p being the cell parameter of the corresponding cubic perovskite) characteristic of the ordered structure of the cuprate [33]. For the compositions x = 5, a disordered rhombohedral perovskite with space group $R\bar{3}c$ is formed, which is in perfect agreement with the already described existence of the pure cobaltites $La_{0.8}Ba_{0.2}CoO_{3-\delta}$ [34] or $La_{0.85}Ba_{0.15}CoO_{3-\delta}$ [35]. When x = 3 and 4, the two phases coexist. Lower values for the solubility limits have been reported in the past for $La_4BaCu_{5-x}M_xO_{13+\delta}$ materials with M = Fe, Ni, Zn and Co, prepared by solid state synthesis at 1000 °C, *i.e.* $x_{Fe} \sim 1$, $x_{Ni} \sim 1.56$, $x_{Zn} \sim 0.47$ and, of particular interest for the present work, $x_{Co} \sim 1.1$ [26]. Alternatively, Co substitution in LBCu matrix has also been obtained up to x = 1 composition *via* synthetic routes using a flux of KOH-NaOH to obtain single crystals [36,37].

The lattice parameters and unit cell volume, obtained from Rietveld refinement using the XRD data, are reported in Table 1. For x = 0, the obtained parameters are in good agreement with those reported previously whatever the synthesis technique [21,24,26,33], *e.g.* $a = 8.644(4)$ Å and $c = 3.867(3)$ Å for Michel et al. prepared by solid state synthesis [33] or $a = 8.6480(1)$ Å and $c = 3.86101(6)$ Å for the more recent report by Macias et al. prepared by the sol-gel technique [21]. The minimum deviation stems from slight differences in the oxygen content that depends on the synthesis method and conditions of preparation, as reported by the different authors; for example, the oxygen stoichiometry of the pure cuprate has been determined as $La_4BaCu_5O_{13.4}$, $La_4BaCu_5O_{12.9}$ or $La_4BaCu_5O_{13.20}$ for Michel et al. [33], Anderson et al. [26], and Shivakumara et al. [24], respectively.

For low Co substitution (x = 1 and 2), the refined cell parameters show a small *a*-axis contraction and *c*-axis expansion, resulting in a limited volume decrease (Table 1). Such results are similar to what was reported by Anderson et al., with $a = b = 8.6094(4)$ Å and

Table 1
Cell parameters of $La_4BaCu_{5-x}Co_xO_{13\pm\delta}$ ($0 \le x \le 5$) compounds obtained from Rietveld refinement using XRD data.

x	Crystal system	Space group	$a = b$ (Å)	c (Å)	V (Å^3)	R_p	R_{wp}	χ^2
0	Tetragonal	*P4/m*	8.6478(2)	3.8605(2)	288.70(1)	4.53	5.97	1.96
1	Tetragonal	*P4/m*	8.6015(9)	3.8830(9)	287.29(6)	4.42	5.55	1.62
2	Tetragonal	*P4/m*	8.6031(1)	3.8853(1)	287.57(7)	3.94	4.99	1.39
3	Tetragonal	*P4/m*	8.6190(1)	3.8792(8)	288.18(7)	2.74	3.48	1.45
	Rhombohedral	$R\bar{3}c$	5.4672(1)	13.314(3)	344.6(1)			
4	Tetragonal	*P4/m*	8.6280(2)	3.8660(1)	287.80(4)	2.55	3.18	1.42
	Rhombohedral	$R\bar{3}c$	5.4694(1)	13.307(3)	344.80(2)			
5	Rhombohedral	$R\bar{3}c$	5.4667(7)	13.27(2)	343.69(8)	3.28	4.16	1.36

c = 3.8861(4) Å for $La_4BaCu_4CoO_{12.98}$; it is worth noting that the same authors couldn't prepare the x = 2 composition as pure phase, probably due to the use of the solid state synthesis route with respect to the sol-gel technique, the latter being more appropriate for complex compositions and structures [26]. The cell parameter evolution with x is in disagreement with the results reported by Shivakumara et al. [36], *i.e.* an increase of the cell volume with both a and c expansion for x = 1. Such discrepancy can be related to the strongly oxidizing medium used by those authors (NaOH–KOH fluxes at 450 °C) with a higher oxygen stoichiometry of $La_4BaCu_4CoO_{13.29}$ and $La_4BaCu_4CoO_{13.35}$, calculated for x = 1 composition by thermogravimetric analysis or iodometric titration, respectively. In the case of x = 5, the obtained parameters are also consistent with reported values for x = 0.2 in $La_{1-x}Ba_xCoO_{3-\delta}$ series [34].

Considering those first results, the rest of our study was dedicated to $La_4BaCu_3Co_2O_{13+\delta}$ (LBCuCo2) composition, as representative member of the fully ordered (with highest Co content) phase since it presents the same tetragonal structure as LBCu.

3.2. Thermal behavior in air

In order to evaluate the structural behavior of LBCuCo2 at high temperature in air and in particular its thermomechanical compatibility with common SOFC electrolytes, thermo-diffraction measurements have been performed from RT to 850 °C. A careful observation of the XRD patterns as a function of temperature shows the absence of extra peaks or change in symmetry in the whole temperature range for the ordered phase (see Fig. S1(a) in supplementary materials). The cell parameters were extracted through LeBail refinement of XRD data using the "cyclic refinement" option of FullProf software [29,30], considering the tetragonal *P4/m* ordered cell indexed to all temperatures. For comparison, the cell parameters were normalized with respect to the perovskite pristine cell, in which $a_p = a/\sqrt{5}$. Fig. 3 shows the evolution of the normalized cell parameters evidencing an almost perfect linear dependence of both parameters with temperature.

The material thermal expansion coefficient (TEC) was calculated considering the following formula in the case of axial tetragonal symmetry [38]:

$$TEC = 1/3\,(2\alpha_a + \alpha_c) \quad (1)$$

where α_a and α_c are the two coefficients of linear expansion normal and along the c-axis, respectively. In this case, values $\alpha_a = 20.2 \times 10^{-6}\,K^{-1}$ and $\alpha_c = 11.3 \times 10^{-6}\,K^{-1}$ were obtained, evidencing an anisotropic thermal expansion, that result in an average TEC value of $17.3 \times 10^{-6}\,K^{-1}$ for LBCuCo2 using Eq. (1). This value is much higher than the typical TEC values for conventional electrolyte materials, *e.g.* 10–11 $\times 10^{-6}\,K^{-1}$ for YSZ ($Zr_{0.85}Y_{0.15}O_{1.925}$), 12–13 $\times 10^{-6}\,K^{-1}$ for GDC ($Ce_{0.9}Gd_{0.1}O_{1.95}$) or 11–12 $\times 10^{-6}\,K^{-1}$ for LSGM ($La_{0.80}Sr_{0.20}Ga_{0.80}Mg_{0.20}O_{3-\delta}$) electrolytes [39–41], what is unfortunately common in cobaltites, *e.g.* $La_{0.7}Sr_{0.3}CoO_{3-\delta}$, $Pr_{0.7}Sr_{0.3}CoO_{3-\delta}$, $SmBa_{0.5}Sr_{0.5}CoCuO_{5+\delta}$ and $La_{0.8}Ba_{0.2}CoO_{3-\delta}$ with TEC of 17.5–19.2 $\times 10^{-6}\,K^{-1}$, 18.8 $\times 10^{-6}\,K^{-1}$ [42], 16.14 $\times 10^{-6}\,K^{-1}$ [20] and 18.2 $\times 10^{-6}\,K^{-1}$ [43], respectively. The high Cu content in LBCuCo2 is not able to mitigate such effect in the material, but it is worth remembering that the pure cuprate itself had a TEC coefficient of 17.3 $\times 10^{-6}\,K^{-1}$ [21], what is, indeed, exactly the same value as for the Co-substituted LBCuCo2 material. Such high TEC value can be considered as an issue for the application as SOFC cathode material for which grading electrode would be a solution, as described in [44] for a similar $La_{0.4}Ba_{0.6}CoO_{3-\delta}$ composition.

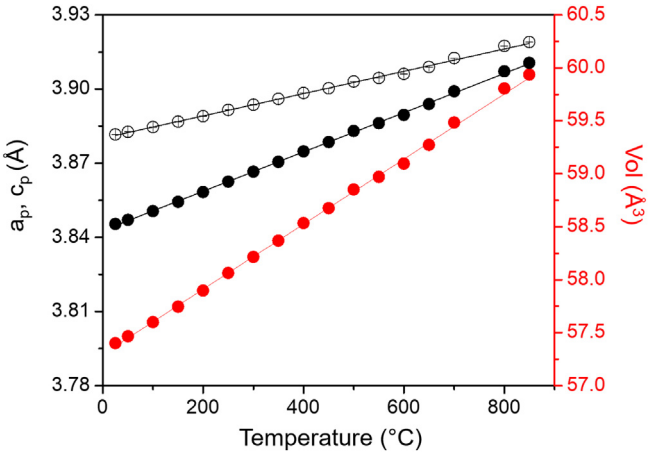

Fig. 3. Evolution of the cell parameters as a function of temperature in air for $La_4BaCu_3Co_2O_{13+\delta}$.

The change of oxygen content up to 800 °C in air for LBCuCo2 was obtained from TGA measurement, considering two consecutive cycles in air shown in Fig. 4 (the first one for desorption of undesirable species). During the first heating in air, the material experiences a major weight loss that corresponds to the desorption of undesirable species. The second cycle presents a weight loss upon heating as a result of the

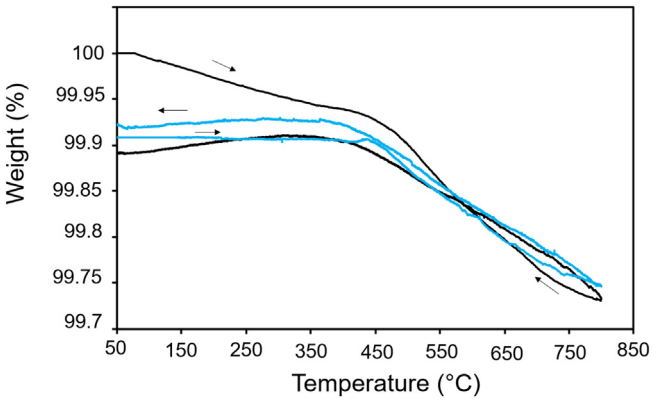

Fig. 4. Thermogravimetric profile for LBCuCo2 in air (black and blue curves for the first and second cycles, respectively). (For interpretation of the references to color in this figure legend, the reader is referred to the web version of this article.)

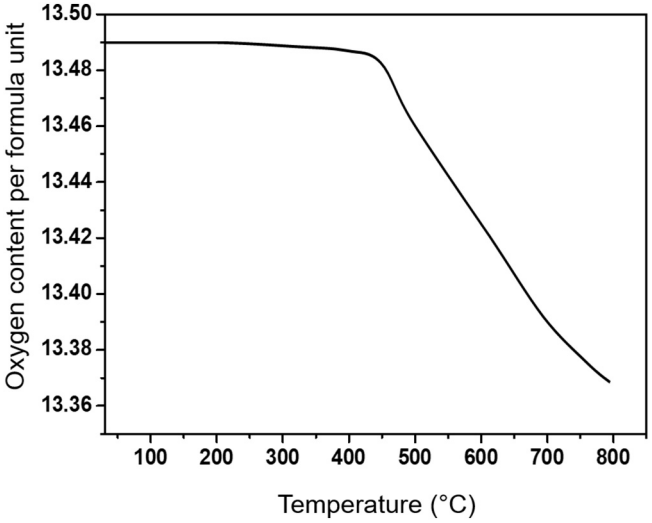

Fig. 5. Variation of the oxygen content as a function of temperature in air for $La_4BaCu_3Co_2O_{13+\delta}$.

loss of oxygen from the crystal lattice. The absolute oxygen content at Room Temperature in air was determined by thermogravimetric titration consisting in a complete sample decomposition in 5% H_2/Ar up to T = 900 °C to form metal (Cu, Co) and binary oxides (La_2O_3 and BaO) (not shown), similarly to what was reported in [24]. From such measurement, the absolute composition of x = 2 material was established as $La_4BaCu_3Co_2O_{13.49}$ after synthesis. Fig. 5 shows the same TGA trace in air of the material during heating but translated in overall oxygen contents. As observed, the oxygen content of $La_4BaCu_3Co_2O_{13+\delta}$ markedly decreases with temperature indicating loss of O atoms from the structure but remains in the range $0.46 \geq \delta \geq 0.37$ for $500 \leq T \leq 800$ °C, the range of temperature of an SOFC, *i.e.* the material still presents a significant concentration of oxygen excess. If we compare to the pure cuprate with quite lower oxygen excess $La_4BaCu_5O_{13.1}$ [21] and $La_4BaCu_4CoO_{13.35}$ [36], it is worth noting the beneficial presence of Co^{3+} in substitution for $Cu^{2+/3+}$ cations that results in a dramatic increase of the oxygen content within the crystal structure, the latter being retained at high temperature.

Neutron diffraction experiments were performed in order to study the oxygen behavior in terms of stoichiometry, *i.e.* vacancy formation, location and, as much as possible, mobility in temperature within $La_4BaCu_3Co_2O_{13+\delta}$ crystal structure. The crystal structure of the compound at room temperature (RT) was investigated using the Rietveld method. Table 2 and Fig. 6 show the final crystal structure parameters and the corresponding graphical result of Rietveld analysis,

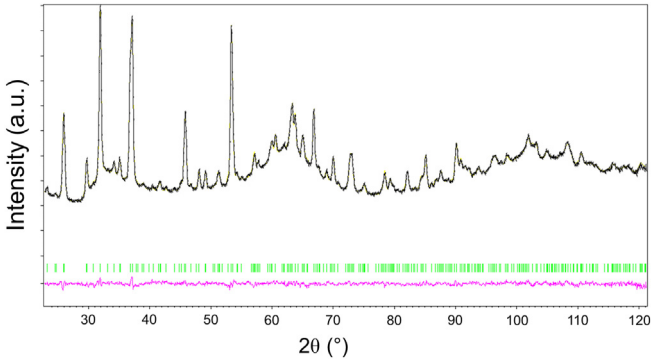

Fig. 6. Graphical result of Rietveld analysis for $La_4BaCu_3Co_2O_{13+\delta}$ using neutron diffraction data at RT (λ = 1.225 Å).

respectively. The main structural feature observed in these results corresponds to the presence of oxygen vacancy rows which are organized around the mixed-valent Cu/Co ions coordinated in square-based pyramids. $La_4BaCu_3Co_2O_{13+\delta}$ is crystallographically equivalent to $La_4BaCu_5O_{13+\delta}$ with a similar distribution of the La and Ba cations, and with the $(Cu/Co)_x$ polyhedra organized in the same framework [37,45]. In order to confirm the occupancy of the Cu/Co cations in the structure, several refinements were performed assuming, in a first stage, the Cu/Co atoms ordered over the four-fold square pyramidal sites (4*j*) in a 3:1 ratio and the Co atoms over the one-fold octahedral sites (1*a*). However, the refinement of the data showed large differences between the corresponding U_{iso} parameters giving values devoid of physical meaning. In this sense, the refinement was addressed considering a mixed occupancy in both sites leaving free to refine the occupancy factors of each cation but keeping the Wyckoff site multiplicity. Following these assumptions, the refinement converged in appropriate structural parameters with acceptable *R*-values. As observed in Table 2, the square-pyramidal sites are occupied by 69% of Cu and 31% of Co while the octahedral sites are occupied by 23% of Cu and 77% of Co. The consideration of mixed cationic 1*a* and 4*j* sites agrees with the results obtained by other neutron diffraction studies on the parent $La_4BaCu_4CoO_{13+\delta}$ composition [26,36]; according to Anderson et al., cobalt occupancies are 45% and 14% of the octahedral and square-pyramidal sites, respectively, against 41% and 15% for Shivakumara et al. [36]. In our case, the Co occupancy of both sites was found higher, in agreement with the higher Co content of the material, but with a clear preference of Co for the octahedral site. In a similar procedure, the presence of oxygen vacancy formation was examined analyzing the tendency of the U_{iso} values through a series of refinements considering all the sites as potential oxygen-deficient sources. The best refinement we obtained, reported in Table 2, corresponds to the case were oxygen

Table 2
Final crystal structure parameters for $La_4BaCu_3Co_2O_{13.47}$ obtained from Rietveld refinement using neutron diffraction data (λ = 1.225 Å).

$La_4BaCu_3Co_2O_{13.47}$
Cell parameters: a = 8.5993(5) Å, c = 3.8800(2) Å, α = β = γ = 90°, V = 286.92(3) Å^3
Space group: *P4/m* (No. 83) - Z = 1
Rp = 1.73; Rwp: 2.24; χ^2 = 1.49

Atom	Site	x; y; z	Uiso (Å^2)*100	Occupancy
Ba1	1d	1/2; 1/2; 1/2	0.44(18)	1.0
La1	4k	0.1171(10); 0.2845(8); 1/2	0.89(15)	1.0
Cu1/Co1	1a	0; 0; 0	0.79(13)	0.23(2)/0.77
Cu2/Co2	4j	0.408(11); 0.1784(8); 0	0.89(10)	0.69(2)/0.31
O1	1b	0; 0; 1/2	1.5(4)	1.0
O2	2e	0; 1/2; 0	1.9(3)	0.235(32)
O3	4j	0.2700(13); 0.3945(13); 0	1.8(3)	1.0
O4	4j	0.2147(13); 0.0646(10); 0	1.4(2)	1.0
O5	4k	0.4136(16); 0.1682(12); 1/2	2.4(4)	1.0

vacancies were exclusively concentrated in the O2(2*e*) sites, *i.e.* within the rows depicted in Fig. 1, what seems not only logical but also observed by Shivakumara et al. [36]. All other attempts considering the presence of oxygen vacancies on other O sites conduce to higher agreement factors or meaningless occupancy (*e.g.* higher than 1). In the case of $La_4BaCu_4CoO_{13+\delta}$, Shivakumara et al. proposed a 5% of vacancy at the site O1 1*b*, at the limit of the precision of the structure refinement [36]; such situation was not confirmed for LBCuCo2, probably due to the higher oxygen stoichiometry of the x = 2 composition of interest. Moreover, it is worth noting the $La_4BaCu_3Co_2O_{13.47}$ stoichiometry obtained from the best solution for Rietveld refinement, in very good agreement with the above discussed oxygen content of the material at RT in air calculated from TG titration in diluted hydrogen (Fig. 5).

To conclude concerning the structure of $La_4BaCu_3Co_2O_{13+\delta}$ material, it is worth noting that, despite the partial disorder of the Cu/Co cation sites, the Co for Cu substitution remains clearly in favor of octahedral occupancy for Co and of square-pyramids for Cu. Together with the specific La/Ba = 4/1 ratio, this is probably the reason why the compound keeps the same oxygen vacancy (Vo) ordering but with an almost one fourth partially filled 2*b* oxygen site, instead of a completely disordered structure on both the La/Ba and Cu/Co sites and incidentally on the atomic position of O/Vo. For higher Co/Cu ratio, *i.e.* for x ≥ 3, the three ordering (at the A and B cation sites as well as the anionic sites of the $ABO_{3-\delta}$ perovskite) disappear at the same time and such structural feature is probably of high importance to understand the oxygen mobility properties of the material series.

3.3. Electrical properties

Fig. 7 shows the evolution of the electrical conductivity of LBCuCo2 as a function of temperature up to 800 °C in air; the inset corresponds to the Arrhenius plot in the low temperature region, where the conductivity is thermally activated. Contrary to the pure cuprate [21], for which a pure metallic-type behavior has been observed in the same temperature range, the conductivity of the Co-doped cuprate presents a semiconductor-type dependence on temperature with an initial value σ = 495 S cm^{-1} at 60 °C that reaches σ = 780 S cm^{-1} at 400 °C. Other materials show such kind of evolution, like the vacancy-ordered $GdBaCo_2O_{5+\delta}$ [46]; in this latter case, the conductivity increases with temperature up to around 450 °C with a very low value of activation energy (E_a ~ 0.02 eV) against E_a = 0.07(1) eV for $La_4BaCu_3Co_2O_{13+\delta}$,

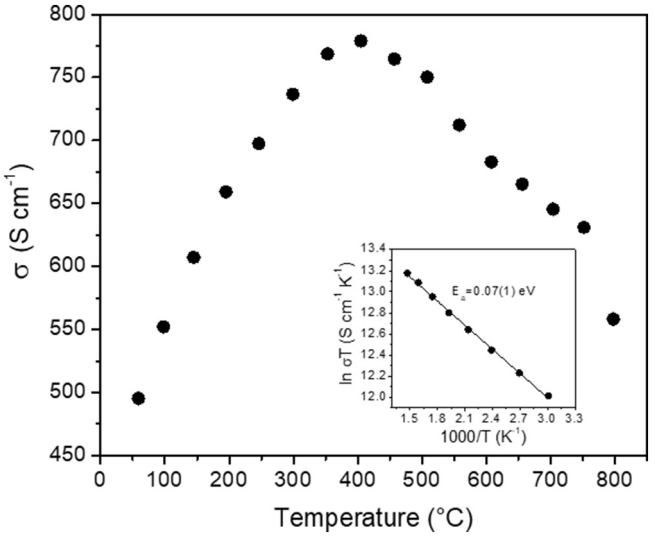

Fig. 7. Temperature dependence in air of electrical conductivity for $La_4BaCu_3Co_2O_{13+\delta}$. In inset, the Arrhenius plot of LBCuCo2 electrical conductivity in the semiconducting region.

explained by a hole (polaronic) mobility [47,48]. Beyond 400 °C, a decrease of the conductivity down to σ = 560 S cm^{-1} at 800 °C is evidenced in LBCuCo2, *i.e.* a metallic-like behavior that seems indeed related to the loss of oxygen observed by TGA (Fig. 5), *i.e.* the reduction of Co^{4+} to Co^{3+}; such trend is similar to what occurs not only in $GdBaCo_2O_{5+\delta}$ [46] but also in $LnBaCo_{2-x}Cu_xO_{5+\delta}$ (Ln = Nd and Gd) series [49–51]. Notwithstanding, LBCuCo2 conductivity values are more than sufficient for the considered application and in good agreement with other authors studies *i.e.* $La_{0.5}Ba_{0.5}CoO_{3-\delta}$ [52], where the transition from a metallic to a semiconducting behavior is observed in the temperature range of an SOFC.

3.4. Electrochemical behavior in air

Fig. 8 shows the IS spectra of LBCuCo2/LSGM/LBCuCo2. The Nyquist and Bode plot collected in air as a function of temperature are presented in Fig. 8(a) and (b), respectively. Fig. 8(c) and (d) show the Nyquist and Bode at 700 °C as a function of the pO_2. The IS data were normalized by the cell area and the symmetrical geometry. The spectra were fitted considering an electrical equivalent circuit consisting of the inductance of the wires (L), in series with the electrolyte resistance (R_{el}) and a resistance (R_1) in parallel with a pseudo-capacitance (CPE_1) corresponding to the electrode response. Table 3 shows the fitting parameters of EIS spectra as a function of Temperature in air and as a function of pO_2 at 700 °C. The R_{el} values are in good agreement with the expected values for a LSGM electrolyte with our geometry by considering the ionic conductivity of this material [53]. Therefore, to facilitate the comparison, the R_{el} was subtracted from the IS spectra in Fig. 8. A second arc appears at low frequency during the measurements as a function of pO_2. This low frequency arc was also fitted with a resistance (R_2) in parallel with a pseudocapacitance (C_2 ~ 0.5–1 F cm^{-2} and p ~ 1, see Table 3). It is worth noting that the high frequency arc was better fitted with the R_1//CPE_1 circuit (C_1 ~ 0.04–0.1 F cm^{-2} and p ~ 0.85, see Table 3) than with the typical Gerischer or Warburg-type impedance associated to O-ion diffusion process. An example of the fitting result is presented in Fig. S2.

Fig. 9(a) shows the Arrhenius plot of the cathode polarization resistance R_P ($R_P = R_1 + R_2$). The R_P decreases from 118 to 0.34 Ω cm^2 when temperature increases from 500 to 750 °C. As a consequence, the activation energy is E_a = 1.65(3) eV. The O_2 reduction mechanism is analyzed based on the behavior of R_P with pO_2. Fig. 9(b) shows the pO_2 dependence of R_1 and R_2. The low frequency resistance R_2, proportional to pO_2^{-1} and with high capacitance value ~0.5–1 F cm^{-2}, can be assigned to the O_2 gas diffusion [54]. As it can be observed from Fig. 9(b), this contribution to the cathode polarization resistance is only relevant at very low pO_2. Therefore, the R_P in air can be referred to the high frequency processes (R_P ~ R_1), which has largest activation energy (1.65 eV) compared with typical values of 1 eV of other lanthanum-barium cobaltites (*e.g.* $La_{0.5}Ba_{0.5}CoO_{3-\delta}$ and $LaBaCo_2O_{6-\delta}$ [55,56]) or lanthanum-barium cuprates (*e.g.* $La_{2-x}Ba_xCuO_{4-\delta}$ [57]). This high activation energy, in addition to the characteristic R//CPE response, the capacitance values and the pO_2 dependence ($pO_2^{-0.38}$) that exhibits the LBCuCo2 electrode, suggest that the O_2 reduction reaction for this material is mainly controlled by a surface process such as O_2 dissociative adsorption or charge transfer process [54,58,59].

4. Conclusion

$La_4BaCu_{5-x}Co_xO_{13+\delta}$ series was synthesized using a modified Pechini route. A change in the oxygen vacancy ordering scheme is evidenced along with the substitution of Co for Cu. When the Co content exceeds 40%, the system turns biphasic with a linear vacancy ordering scheme similar to the pure cuprate found for x ≤ 2 and a disordered perovskite phase. For x = 5, the material is a pure rhombohedral perovskite. $La_4BaCu_3Co_2O_{13+\delta}$, however, presents much higher oxygen excess δ than the non-doped cuprate. TGA and Neutron

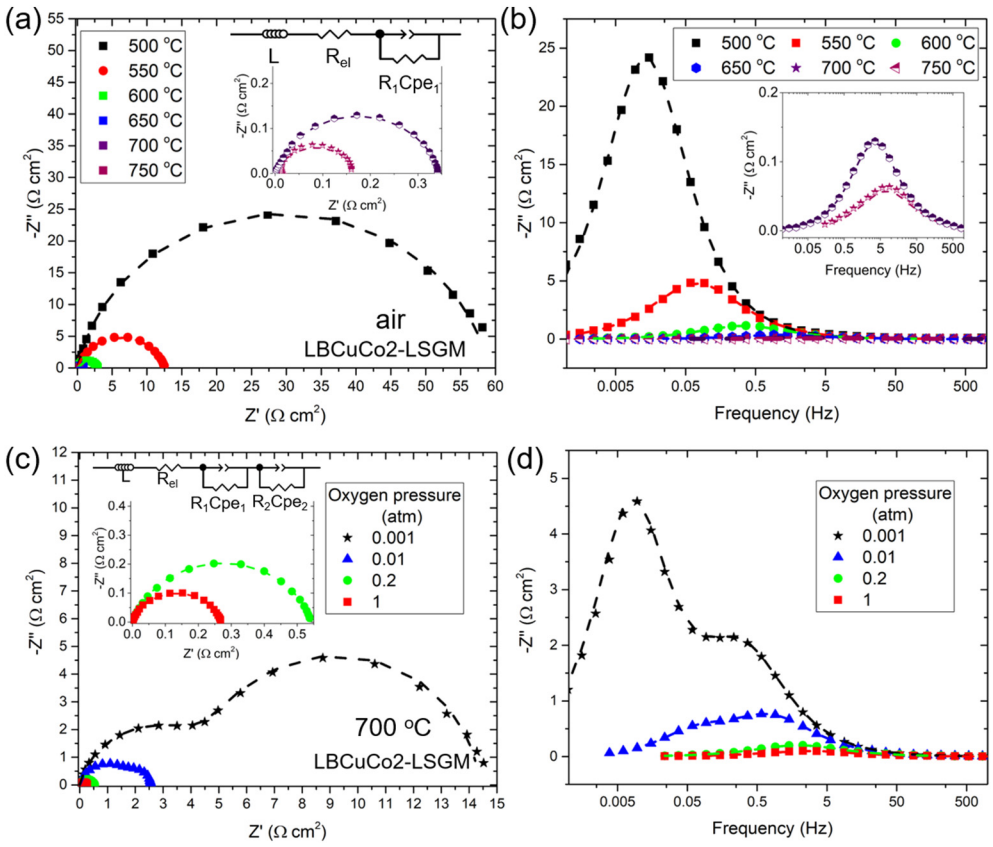

Fig. 8. Impedance spectra of porous $La_4BaCu_3Co_2O_{13+\delta}$ electrode deposited on LSGM electrolyte (LBCuCo2/LSGM/LBCuCo2). (a) Nyquist and (b) Bode plots collected in air as a function of temperature; (c) Nyquist and (d) Bode plots collected at 700 °C as a function of the pO_2. Dashed lines correspond to the fitted results with the electrical equivalent circuit indicated inside the graphs.

Table 3
EIS fitting parameters of $La_4BaCu_{0.3}Co_{0.2}O_{13\pm\delta}$ electrode on LSGM electrolyte obtained from the electrical equivalent circuit.

T (°C)	pO_2 (atm)	R_{el} (Ωcm)	R_1 (Ωcm^2)	CPE_1 (Fcm^{-2})	p	f_{max1} (Hz)	R_2 (Ωcm^2)	CPE_2 (Fcm^{-2})	p	f_{max2} (Hz)	χ^2
500	0.2	615(1)	118.0(5)	0.0404(2)	0.879(2)	0.027					1.8×10^{-4}
550	0.2	284(1)	25.1(1)	0.0429(4)	0.833(5)	0.146					9.0×10^{-4}
600	0.2	156.8(1)	5.84(1)	0.0504(3)	0.848(2)	0.674					7.7×10^{-5}
650	0.2	105.7(1)	1.853(5)	0.0557(5)	0.840(3)	2.379					6.7×10^{-5}
700	0.2	82.8(1)	0.692(2)	0.067(1)	0.809(4)	7.039					3.8×10^{-5}
750	0.2	66.4(1)	0.34(1)	0.098(1)	0.75(2)	14.77					3.8×10^{-4}
700	1	82.902(1)	0.542(2)	0.104(2)	0.807(5)	5.613					5.1×10^{-5}
700	0.24	85.115(2)	1.080(3)	0.0656(6)	0.825(3)	3.946					2.5×10^{-5}
700	9.8×10^{-3}	90.223(2)	3.58(3)	0.0402(3)	0.846(2)	1.575	1.55(3)	0.80(3)	0.98(1)	0.128	1.8×10^{-5}
700	6.9×10^{-4}	94.241(8)	9.3(1)	0.0336(4)	0.846(5)	0.633	19.5(2)	0.45(1)	0.95(1)	0.016	2.5×10^{-4}

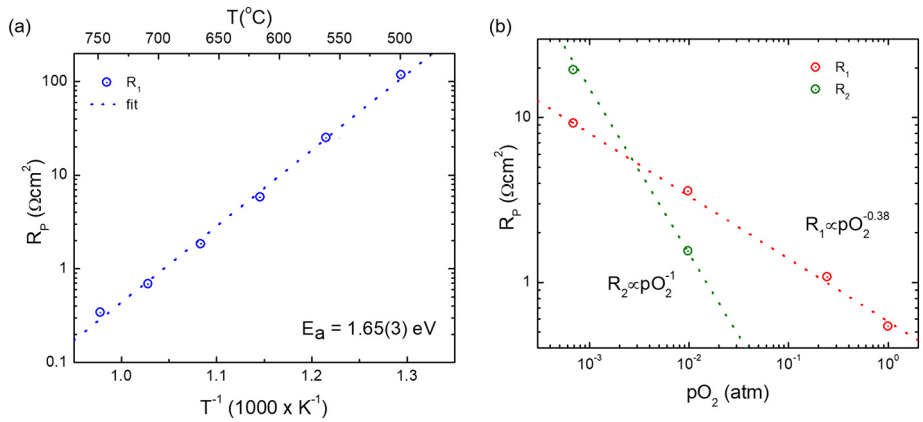

Fig. 9. (a) Arrhenius plot of the LBCuCo2 cathode polarization resistance R_P. The activation energy is indicated inside the graph. (b) log-log plot showing the pO_2 dependence of R_1 and R_2. Dashed lines correspond to the fitted results.

Diffraction measurements are consistent and confirm that the oxygen excess is located in vacant sites; δ remains high even beyond 600 °C, being promising in view of the desired MIEC properties. Despite the high TEC coefficient, LBCuCo2 exhibits high values of electrical conductivity (between 560 and 680 S cm^{-1} in the range 600–800 °C), more than sufficient for the application as SOFC cathode. The LBCuCo2 electrodes reaches a $R_P = 0.34\ \Omega\ cm^2$ in air at T = 750 °C making these materials suitable for IT-SOFC.

Supplementary data to this article can be found online at https://doi.org/10.1016/j.ssi.2018.10.001.

Acknowledgements

The authors acknowledge the financial support of UIS' Vicerrectorship for Investigation and Extension (Project #1801), CNRS, Région Nord Pas-de-Calais and European Regional Development fund. This research used resources of the Brazilian Synchrotron Light Laboratory (LNLS), an open national facility operated by the Brazilian Centre for Research in Energy and Materials (CNPEM) for the Brazilian Ministry for Science, Technology, Innovations and Communications (MCTIC). The D10B-XPD beamline staff is acknowledged for the assistance during the initial characterization experiments of the samples studied in this work under proposal #15297. The authors are grateful to Dr. Florence Porcher from LLB-Saclay-France for neutron powder diffraction measurements, to Prof. Konrad Świerczek from AGH for the High Temperature X Ray Diffraction measurements and fruitful discussion and to the Laboratorio de Difracción de Rayos X (Parque Tecnológico Guatiguará-UIS) for X-Ray Diffraction measurements at RT. Silvia Durán, Mónica V. Sandoval and Mario A. Macías are grateful to UIS and COLCIENCIAS for their respective scholarships. Mario A. Macías and Jhoan Téllez are also grateful to ANII-Uruguay for offering them, respectively, a post-doctoral scholarship #PD-NAC 2014_1_102409 and a partial financial support during the stay in Uruguay (#PR_FSE_2013_10689).

References

[1] W. He, W. Lu, J. Dickerson, Gas Transport in Solid Oxide Fuel Cells, SpringerBriefs, USA, 2014.
[2] J.T.S. Irvine, P. Connor, Solid Oxide Fuel Cells: Facts and Figures, Springer – Verlag, London, 2013.
[3] C. Sun, U. Stimming, J. Power Sources 171 (2007) 247–260.
[4] Y.H. Huang, R.I. Dass, Z.L. Zing, J.B. Goodenough, Science 312 (2006) 254–257.
[5] C. Xia, W. Rauch, F. Chen, M. Liu, Solid State Ionics 149 (2002) 11–19.
[6] S. Park, S. Choi, J. Shin, G. Kim, J. Power Sources 210 (2012) 172–177.
[7] K.T. Lee, A. Manthiram, J. Electrochem. Soc. 152 (2005) A197–A204.
[8] O. Gwon, S. Yoo, J. Shin, G. Kim, Int. J. Hydrog. Energy 39 (2014) 20806–20811.
[9] Y. Teraoka, H.M. Zhang, K. Okamoto, N. Yamazoe, Mater. Res. Bull. 23 (1988) 51–58.
[10] Z. Shao, S.M. Haile, Nature 431 (2004) 170–173.
[11] K. Efimov, Q. Xu, A. Feldhoff, Chem. Mater. 22 (2010) 5866–5875.
[12] S. Choi, S. Park, J. Kim, T.-H. Lim, J. Shin, G. Kim, Electrochem. Commun. 34 (2013) 5–8.
[13] S. Pang, X. Jiang, X. Li, Z. Su, H. Xu, Q. Xu, C. Chen, Int. J. Hydrog. Energy 37 (2012) 6836–6843.
[14] N. Li, Z. Lü, B. Wei, X. Huang, K. Chen, Y. Zhang, W. Su, J. Alloys Compd. 454 (2008) 274–279.
[15] K. Zhang, L. Ge, R. Ran, Z. Shao, S. Liu, Acta Mater. 56 (2008) 4876–4889.
[16] D. Chen, R. Ran, K. Zhang, J. Wang, Z. Shao, J. Power Sources 188 (2009) 96–105.
[17] X. Che, Y. Shen, H. Li, T. He, J. Power Sources 222 (2013) 288–293.
[18] F. Jin, H. Xu, W. Long, Y. Shen, T. He, J. Power Sources 243 (2013) 10–18.
[19] S. Lü, G. Long, Y. Ji, X. Meng, H. Zhao, C. Sun, J. Alloys Compd. 509 (2011) 2824–2828.
[20] B. Wang, G. Long, Y. Li, Y. Ji, Int. J. Hydrog. Energy 41 (2016) 13603–13610.
[21] M.A. Macias, M.V. Sandoval, N.G. Martinez, S. Vázquez-Cuadriello, L. Suescun, P. Roussel, K. Świerczek, G.H. Gauthier, Solid State Ionics 288 (2016) 68–75.
[22] A. Kopp Alves, C.P. Bergmann, F.A. Berutti, Novel Synthesis and Characterization of Nanostructured Materials, Springer, Brazil, 2013.
[23] M. Kakihana, J. Sol-Gel Sci. Technol. 6 (1996) 7–55.
[24] C. Shivakumara, ISRN Ceram. 2011 (2011) 859385.
[25] X.H. Huang, H. Chen, T.T. Wu, Adv. Mater. Res. 66 (2009) 57–60.
[26] P.S. Anderson, C.A. Kirk, J.M.S. Skakle, A.R. West, J. Solid State Chem. 170 (2003) 1–8.
[27] M. Galceran, M.C. Pujol, M. Aguiló, F. Díaz, J. Sol-Gel Sci. Technol. 42 (2007) 79–88.
[28] X. Zhang, J. Zhou, Y. Wang, Ionics 19 (2013) 941–945.
[29] J. Rodríguez-Carvajal, Phys. B Condens. Matter 192 (1993) 55–69.
[30] J. Rodríguez-Carvajal, WinPLOTR, Commission Powder Diffr. Newsl, vol. 26, 2001, pp. 12–19.
[31] L. P, V. Petricek, M. Dusek, JANA2006, (2006).
[32] D. S, M. Zahid, I. Arul Raj, F. Tietz, P. Lersch, Proc. - Electrochem. Soc. PV 2005–07 (2005) 1708–1716.
[33] C. Michel, L. Er-Rakho, B. Raveau, Mater. Res. Bull. 20 (1985) 667–671.
[34] C. Setevich, L. Mogni, A. Caneiro, F. Prado, J. Electrochem. Soc. 159 (2012) B73–B80.
[35] W. Luo, F. Wang, Powder Diffract. 21 (2006) 304–306.
[36] C. Shivakumara, M.S. Hegde, H. Rajagopal, A. Sequiera, Mater. Res. Bull. 35 (2000) 2063–2068.
[37] C. Shivakumara, M.S. Hegde, S. Prakash, G.N. Subbanna, N.P. Lalla, J. Mater. Chem. 8 (1998) 2695–2700.
[38] R.E. Taylor, C.Y. Ho, Thermal Expansion of Solids, ASM International, Materials Park (OH), USA, 1998.
[39] G.A. Tompsett, N.M. Sammes, O. Yamamoto, J. Am. Ceram. Soc. 80 (1997) 3181–3186.
[40] H. Hayashi, T. Saitou, N. Maruyama, H. Inaba, K. Kawamura, M. Mori, Solid State Ionics 176 (2005) 613–619.
[41] Z. Naiqing, S. Kening, Z. Derui, J. Dechang, J. Rare Earths 24 ((2006) 90–92.
[42] F. Tietz, Ionics 5 (1999) 129–139.
[43] C. Martínez, Propiedades de las perovskitas ABO_3 (A = La,Ba y B = Co,Fe) como material de catodo en celdas de combustible IT-SOFC, Universidad Nacional del Sur, 2014.
[44] C.F. Setevich, L.V. Mogni, A. Caneiro, F.D. Prado, Int. J. Hydrog. Energy 37 (2012) 14895–14901.
[45] N. Rangavittal, G.N. Subbanna, T.N.G. Row, C.N.R. Rao, J. Solid State Chem. 114 (1995) 95–101.
[46] A. Tarancón, D. Marrero-lópez, J. Peña-martínez, J.C. Ruiz-morales, P. Núñez, Solid State Ionics 179 (2008) 611–618.
[47] S. Streule, A. Podlesnyak, D. Sheptyakov, E. Pomjakushina, M. Stingaciu, K. Conder, M. Medarde, M.V. Patrakeev, I.A. Leonidov, V.L. Kozhevnikov, J. Mesot, Phys. Rev. B 73 (2006) 1–5.
[48] E. Mitberg, Solid State Ionics 130 (2000) 325–330.
[49] J.H. Kim, A. Manthiram, J. Mater. Chem. A 3 (2015) 24195–24210.
[50] Y.N. Kim, A. Manthiram, J. Electrochem. Soc. 158 (2011) B276–B282.
[51] J.-H. Kim, A. Manthiram, J. Electrochem. Soc. 155 (2008) B385–B390.
[52] R. Amin, K. Karan, J. Electrochem. Soc. 157 (2010) B285–B291.
[53] K. Huang, J.B. Goodenough, J. Alloys Compd. 303–304 (2000) 454–464.
[54] S. Adler, Chem. Rev. 104 (2004) 4791–4844.
[55] D. Garcés, H. Wang, S.A. Barnett, A.G. Leyva, F.R. Napolitano, R.O. Fuentes, H.E. Troiani, L.V. Mogni, J. Mater. Chem. A 6 (2018) 16699–16709.
[56] D. Garcés, A.L. Soldati, H. Troiani, A. Montenegro-Hernández, A. Caneiro, L.V. Mogni, Electrochim. Acta 215 (2016) 637–646.
[57] A. Niemczyk, A. Olszewska, Z. Du, Z. Zhang, K. Świerczek, H. Zhao, Int. J. Hydrog. Energy (2018) 1–13.
[58] S.B. Adler, X.Y. Chen, J.R. Wilson, J. Catal. 245 (2007) 91–109.
[59] S. Miyoshi, A. Takeshita, S. Okada, S. Yamaguchi, Solid State Ionics 285 (2016) 202–208.